

Evaluation of energy spectrum around structural materials in radiation environments



Taichi Matsumura^{a,*}, Ryuji Nagaishi^a, Jun-ichi Katakura^b, Masahide Suzuki^b

^a Japan Atomic Energy Agency, 2-4 Shirakata, Tokai-mura, Naka-gun, Ibaraki-ken, 319-1195, Japan

^b Nagaoka University of Technology, 1603-1, Kamitomioka Nagaoka, Niigata, 940-2188, Japan

ARTICLE INFO

Keywords:

SUS304

Gamma-ray

Beta-ray

Secondary radiation

Energy spectrum

ABSTRACT

Structural materials such as stainless steel (SUS) in nuclear reactor are exposed by the environment of ionizing radiations so that their corrosion and degradation take place. These radiation effects depend strongly on the quality of radiation (energy, kind) around the materials. The metallic materials with various thickness have been examined in previous works on the radiation effects, but not with a common thickness. The different thickness would give the different radiation quality, leading to the different results of radiation effects on the materials. In this work, when radiation sources of ^{137}Cs , ^{90}Sr and ^{90}Y were assumed to be put in the front of a plain SUS304 plate as a typical material submerged in water, energy spectra of secondary photons and electrons at the front and back sides of plate were simulated with changing the thickness of plate, and spacing between the source and plate by using a Monte Carlo calculation code of PHITS.

In the case of ^{137}Cs gamma-ray (monochromatic 662 keV), the energy spectra at the front side was smaller than those at the back side due to the existence of plate. Then the dependence of spectra on the plate thickness was observed more clearly at the back side than at the front side. In the cases of ^{90}Sr and ^{90}Y beta-rays (maximum 546 and 2284 keV), the energy spectra were clearly different from those in the case of gamma-ray. At the front side, the energy and flux of electrons were higher than those of photons. Also, the energy spectra of electrons and photons were not dependent on the plate thickness. At the back side, the energy and flux of electrons were much lower than those of photons reversely. It was clearly shown how the energy spectra of photons and electrons varied with the incident radiation type, the spacing, and the thickness.

The average energies of secondary radiations were further estimated, and the changes of incident radiation to the secondary ones were discussed especially in terms of the lowering of radiation energy.

1. Introduction

Since metallic structural materials in nuclear reactor are placed in the environment of radiations, their corrosion and degradation occur. These radiation effects depend on the quality of radiation around the materials. The radiation quality such as linear energy transfer (LET) is determined by the type and energy of radiation. The quality further depends on the kind and thickness of structural material. Generally, the effect has been evaluated based on the dose given by primary and incident radiation. But the incident radiation interacts with the materials and then its quality changes. So, it is important to take this change into consideration for the evaluation of effects.

Radiations that affects the materials at the loss-of-coolant accident (LOCA) are mainly gamma (γ)- and beta (β)-rays emitted from ^{137}Cs ,

^{90}Sr , and ^{90}Y which are major radionuclides (Okumura et al., 2013) as seen in Fukushima Dai-ichi Nuclear Power Station (1F) (Nagaishi et al., 2014). γ -ray is a type of electromagnetic waves with monochromatic energies and interacts with matter through photoelectric effect, Compton scattering, and electron pair production to generate secondary electrons as well as scattered photons. On the other hand, β -ray (minus) as an electron is emitted with a continuous energy distribution. The electrons are fairly influenced by atomic coulomb fields in matter because they are very light compared to other charged particles (e.g. proton). Therefore, β -ray strongly interacts with matter, and is quickly decelerated and absorbed by matter. When γ - and β -ray interact with matter, the primary radiations become secondary radiations of photons and electrons with lower and continuous energy so that the quality of radiations depends on matter. Therefore, it is important to evaluate the

* Corresponding author.

E-mail addresses: matsumura.taichi@jaea.go.jp (T. Matsumura), nagaishi.ryuji@jaea.go.jp (R. Nagaishi), j.katakura@vos.nagaokaut.ac.jp (J.-i. Katakura), suzuki.masahide@vos.nagaokaut.ac.jp (M. Suzuki).

<https://doi.org/10.1016/j.radphyschem.2019.108493>

Received 17 May 2019; Received in revised form 9 September 2019; Accepted 12 September 2019

Available online 15 September 2019

0969-806X/© 2019 Elsevier Ltd. All rights reserved.

quality of secondary radiations around the structural material for evaluating its radiation effects as well as the quantity.

In the research field of radiation chemistry, primary yields (G-values) of radiolysis products of water are well known to strongly depend on LET (or stopping power) (Allen, 1961). The secondary radiations of lower and continuous energies give higher LET than the primary one before interacted. So, the G-values for the secondary radiations would be different from those for the primary one. Currently in works on the radiation effects of materials, they have been examined with various thickness, but not with a common thickness. The material of different thickness would give the different energy spectra of secondary radiations especially around the material.

In this work, when radiation sources of ^{137}Cs , ^{90}Sr and ^{90}Y were assumed to be put in the front of a plain SUS304 plate as a typical material submerged in water, the energy spectra of secondary photons and electrons at the front and back sides of plate were simulated with changing the thickness of plate, and the spacing between the source and plate by using a Monte Carlo calculation code of the Particle and Heavy Ion Transport Code System (PHITS) (Sato et al., 2018). In these simulations, the following four items were examined and discussed.

- (1) Analysis of energy spectra of secondary radiations of photons and electrons generated from SUS304 and water by their interaction with γ -rays from ^{137}Cs (3.1.1)
- (2) The estimation of average energies of secondary radiations generated from SUS304 and water by their interaction with γ -rays from ^{137}Cs (3.1.2)
- (3) Analysis of energy spectra of secondary radiations of photons and electrons generated from SUS304 and water by their interaction with β -rays from ^{90}Sr and ^{90}Y (3.2.1)
- (4) The estimation of average energies of secondary radiations generated from SUS304 and water by their interaction with β -rays from ^{90}Sr and ^{90}Y (3.2.2)

The main component of structural materials such as stainless steel (SUS) is iron. So SUS304 was used as a typical material in this work.

2. Calculation procedure

2.1. Determination of calculation condition

In this subsection, three parts important for calculation were determined at fast: (1) thickness of observation region, (2) spacing between radiation source and SUS304, and (3) observed surface area of SUS304.

In the first part, the thickness of observation region was determined in the followings. In water radiolysis, hydrogen peroxide (H_2O_2) is formed as a molecular product and generally acts as an oxidizing agent for the corrosion and degradation of structural materials (Hanawa et al., 2010). On the other hand, it is known that H_2O_2 is thermally (self) decomposed ($\text{H}_2\text{O}_2 \rightarrow \text{H}_2\text{O} + 1/2\text{O}_2$) under conditions of high temperature (Takagi et al., 1985) and catalyst contact. Thus, the reachable range of H_2O_2 which can be involved in the oxidation of materials would be determined from a relation between the decay rate, k and diffusion coefficient, D of H_2O_2 . In preliminary experiments, the decomposition rates were obtained at room temperature (298 K) with changing pH and with addition of solids such as MnO_2 and zeolites.

Fig. 1 roughly shows the relationship between the H_2O_2 decay rate, k (reciprocal of lifetime, τ) and diffusion length, L at 298 K. The one-dimensional L can be calculated from k and D ($L = \sqrt{2\pi D\tau}$). The measured k ($10^{-3} \sim 10^{-2} \text{ s}^{-1}$) in the presence of the solids at 298 K was comparable to the reported value (J. Takagi et al., 1985 (Itoh, 1988)) in aqueous solutions at high temperature (423–473 K). When it is assumed that H_2O_2 do not react with any solutes, the influence range for the radiation effects of materials was evaluated as the linear diffusion length of H_2O_2 with its lifetime. In the case of zeolites loaded in the

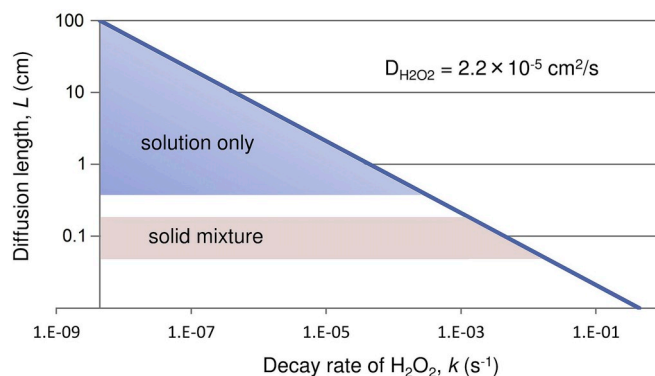


Fig. 1. Relationship between lifetime (reciprocal of speed) and diffusion length of H_2O_2 at 298 K.

adsorption vessel used for the decontamination of radioactive water (Matsumura et al., 2018), the range became much shorter than 1 cm. From this range and range of β -ray in water as described below, the thickness of observation region was determined to be 1 mm in the work.

In this second part, the spacing between radiation source and SUS304 was determined in the followings. Since γ -ray is of high transparency, the position of γ -ray source was determined based on the position of β -ray source. Table 1 shows the energies of γ -ray and β -rays emitted from the major radionuclides of ^{137}Cs , ^{90}Sr and ^{90}Y . Table 2 shows mean free path (MFP) and continuous slowing down approximation (CSDA) ranges in water and SUS304. The monochromatic energy of γ -ray emitted from ^{137}Cs is 662 keV (Katakura et al., 2016). From the linear attenuation coefficient (Hubbell et al., 1995), MFP in water is 116 mm. β -rays emitted from radionuclides have continuous energy distributions. The average energies become considerably smaller than the maximum ones. The CSDA ranges of β -rays in water and SUS304 can be estimated from NIST's ESTAR program (NIST Physical Measurement Laboratory (ESTAR program)). The CSDA range can be obtained by integrating the reciprocal of the total stopping power with respect to energy. When the energy of electron is 196 keV, the CSDA range in water is 0.044 g/cm². Water density is 1.0 g/cm³ (T. Sato et al., 2018). Therefore, maximum range is 0.44 mm. The range of 934 keV in water is 0.402 g/cm² (4.02 mm). Since ^{90}Y is a daughter nuclide of ^{90}Sr , it was assumed that it exists at the same place as ^{90}Sr . From the above data, the spacing between the radiation source and SUS304 was determined to be 0.0, 0.5, and 1.0 mm.

In this third part, the surface area of SUS304 was determined in the followings. Since seawater was injected at the 1F accident, the corrosion of SUS in the presence of chloride ion in the seawater is mainly pitting one (John Sedriks et al., 1979). The pitting corrosion test in Japan is conducted with test pieces of 100 mm \times 150 mm and 20 mm \times 30 mm according to JIS G 0577, 0578 and 0590 (JIS G 0577: 2014 (JIS G 0577, 2014); JIS G 0578: 2013 (JIS G 0578, 2013); JIS G 0590: 2013 (JIS G 0590, 2013)). In the tests, a surface area of

Table 1

Energy of gamma and beta-rays emitted from radioactive nuclides (Katakura et al., 2016; Eckerman et al., 1994).

Radioactive nuclide		^{137}Cs ($^{137\text{m}}\text{Ba}$)	^{90}Sr	^{90}Y
Radiation (quality)		γ	β^-	β^-
Energy (keV)	maximum	662	546	2284
	average		196	934
Recoiled electron (keV)	Radiation (quality)	e	-	-
	maximum ^a	478		
	average ^b	253		

^a Maximum energy at Compton edge.

^b Obtained from average energy of Compton-scattered photon.

Table 2

Mean free path (MFP) and continuous slowing down approximation (CSDA) range of water and SUS304 (Katakura et al., 2016; Hubbell et al., 1995); NIST Physical Measurement Laboratory (ESTAR program; (Eckerman et al., 1994).

energy (keV)		MFP (mm)		CSDA range (g/cm ²)		
		Water	SUS304	Water	SUS304	SUS304
662	γ -ray	662	–	–	–	–
–	β -ray	–	196	546	934	2284
Water		116	0.044	0.200	0.402	1.129
SUS304		16.8	0.065	0.289	0.573	1.551

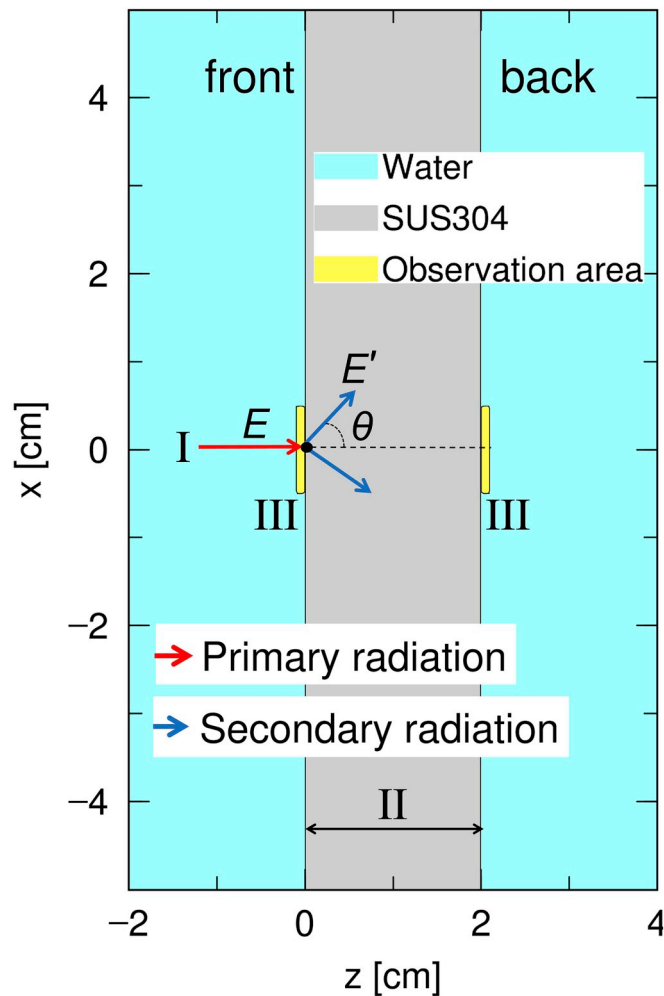


Fig. 2. Conceptual diagram of analysis conditions. I. Position of the radiation source from the structural material: 0.0, 0.5, 1.0 mm respectively. ⁹⁰Sr was set at the position of 0.0, 0.5 mm because of its CSDA range in water. II. Thickness of structural material: 1 mm, 2 mm, then set to 20 mm in steps of 2 mm. III. Observation area of energy spectrum of photons and electrons of secondary radiation: the observation area was set in the area of 10 mm × 10 mm × 1 mm on the X, Y and Z axes of both of the front and back sides of structural material.

10 mm × 10 mm in the test pieces is taken and defined as a measurement area (JIS G 0577: 2014 (JIS G 0577, 2014); JIS G 0578: 2013 (JIS G 0578, 2013); JIS G 0590: 2013 (JIS G 0590, 2013)). From these tests, the observed surface area of SUS304 was define to be 1.0 cm² (10 mm × 10 mm).

Finally, the calculation conditions were set as schematically shown in Fig. 2. The SUS304 plate was placed in water. The irradiation position (I in Fig. 2) of primary radiation was set within 1.0 mm from SUS304. Therefore, three positions of 1.0 mm, 0.5 mm and 0.0 mm from SUS304 were selected. Only ⁹⁰Sr was set at the position of 0.0, 0.5 mm according to the CSDA range in water. As described above in the

corrosion test, the test surface of 10 mm × 10 mm was assumed to be the observed area. Therefore, the shape of SUS304 was a square of 100 mm × 100 mm in the X, Y axis directions and had a surface sufficiently larger than the observed area. Then, when the energy spectra of photons and electrons were simulated in water at the front and back sides of the SUS304, the thickness of SUS304 was changed from 1 mm to 20 mm (II in Fig. 2).

The virtual detector of T-Track in the PHITS simulation was set at the observation area (III in Fig. 2) of 10 mm × 10 mm × 1 mm in the X, Y, Z-axis directions centering on the origin of SUS304. The T-Track obtained the fluences of photons and electrons in the specified region. The energy range in the simulation was 5–2400 keV. The radiations emitted from the radionuclides at the front side were assumed to irradiate to SUS304 vertically without isotropic irradiation, and then the angle was defined as $\theta = 0^\circ$.

2.2. Material

The Compositions and densities of SUS304 and water used in this work were referred from the material composition table in PHITS (Sato et al., 2018). The structural material was SUS304. The density was 8.03 g/cm³ (Sato et al., 2018). The relative amounts of atom by weight in SUS304 were C 4.82E-3, Si 6.42E-2, P 3.21E-3, S 1.61E-3, Cr 1.53E+0, Mn 1.45E-1, Fe 5.55 E+0, and Ni 7.39E-1. The surroundings of SUS304 was water. The density was 1.0 g/cm³ (Sato et al., 2018). The relative amounts of atom by weight in water were H 1.12E-1 and O 8.88E-1.

2.3. Radiation sources

γ -ray emitted from ¹³⁷Cs (^{137m}Ba) has a monochromatic energy of 662 keV (Katakura et al., 2016). β -rays emitted from ⁹⁰Sr and ⁹⁰Y have energy distributions with maximum energies of 546 and 2284 keV (Eckerman et al., 1994).

2.4. Photons, electrons and positrons cross-section libraries and re-try number and precision (statistical error)

Photons cross-section and library are available from Klein-Nishina cross-section (Klein et al., 1929), Bethe-Heitler cross-section (Bethe et al., 1934) and PHOTX library (Radiation Shielding Information Center, Oak Ridge National Laboratory, 1995 (PHOTX, 1995)). Electrons and Positrons cross-section are from Bethe-Heitler cross-section (Heitler et al., 1954) and Heitler cross-section (W. Heitler et al., 1954 (Farhataziz et al., 1987)).

Re-try number was 4.0 E+7 in this work. The numbers after \pm were values of statistical errors obtained from the re-try number of PHITS Monte Carlo simulation.

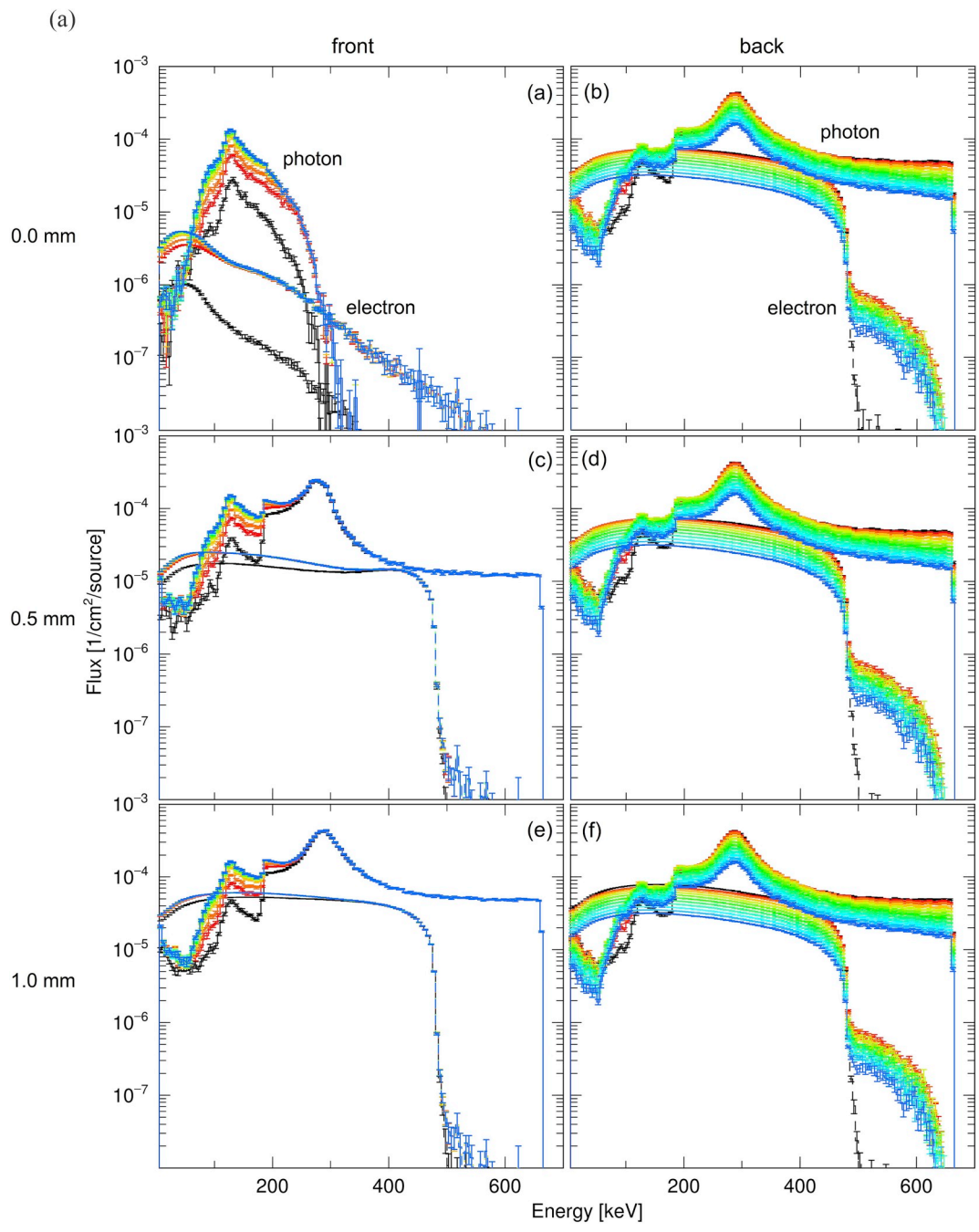
3. Results and discussion

3.1. Simulated calculation with ¹³⁷Cs γ -ray irradiation

3.1.1. Energy spectrum with γ -ray irradiation

Fig. 3a shows that the spectra of secondary radiations of photons and electrons were calculated at the front and back sides of SUS304 with changing the spacing and thickness indicated in Fig. 3b. The shapes of spectra were irrespective of the existence of SUS304. In order to observe the shape changing clearly, the spectra were shown at the fixed thickness of SUS304 (1 mm) in Fig. 4. However, the shapes significantly changed with the spacing.

At the front side of SUS304, a photon peak under any conditions could be seen in the energy region of 125–135 keV, in which the weighted center (average energy) was obtained from Fig. 3a (a) and Fig. 4 (a) to be 148 ± 22.2 to 157 ± 18.7 keV. The numbers after \pm were values of statistical errors obtained from the re-try



(b)













color	mm	color	mm
	0		10
	1		12
	2		14
	4		16
	6		18
	8		20

Fig. 3. (a). Dependence of energy spectra of secondary radiations in water on SUS304 thickness, and on spacing between gamma-ray source of ^{137}Cs and SUS304. (a), (c), and (e) were the front side at the spacing of 0.0 mm, 0.5 mm and 1.0 mm, respectively. (b), (d), and (f) were the back side at 0.0 mm, 0.5 mm and 1.0 mm, respectively. The solid line denotes photon, and the dashed line electron. (3b). Correspondence table between thickness of SUS304 and color. . (For interpretation of the references to color in this figure legend, the reader is referred to the Web version of this article.)

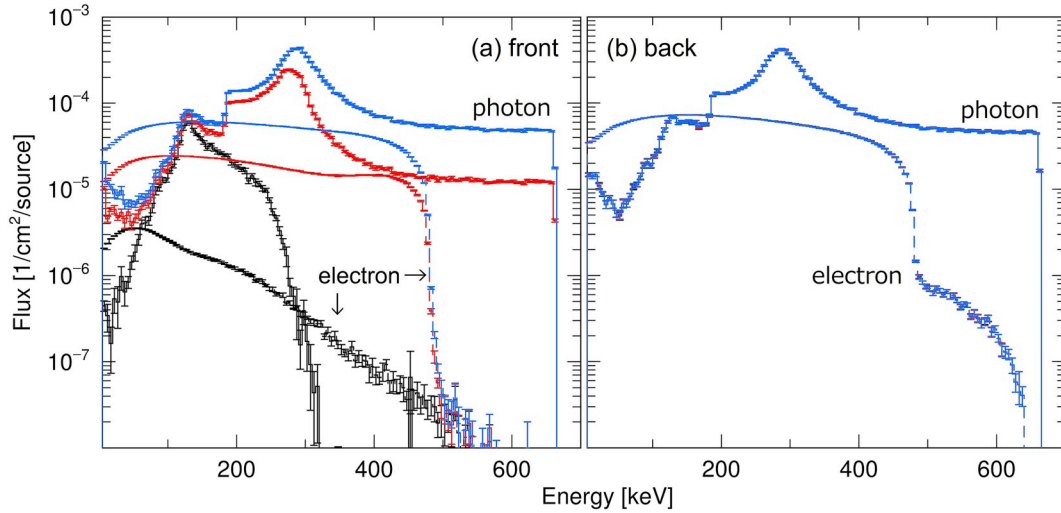


Fig. 4. Dependence of energy spectra of secondary radiations at a fixed SUS304 thickness of 1 mm on spacing between gamma-ray source of ^{137}Cs and SUS304. The solid line denotes photon, and the dashed line electron. The black line denotes 0.0 mm spacing, the red line 0.5 mm, and the blue line 1.0 mm. (For interpretation of the references to color in this figure legend, the reader is referred to the Web version of this article.)

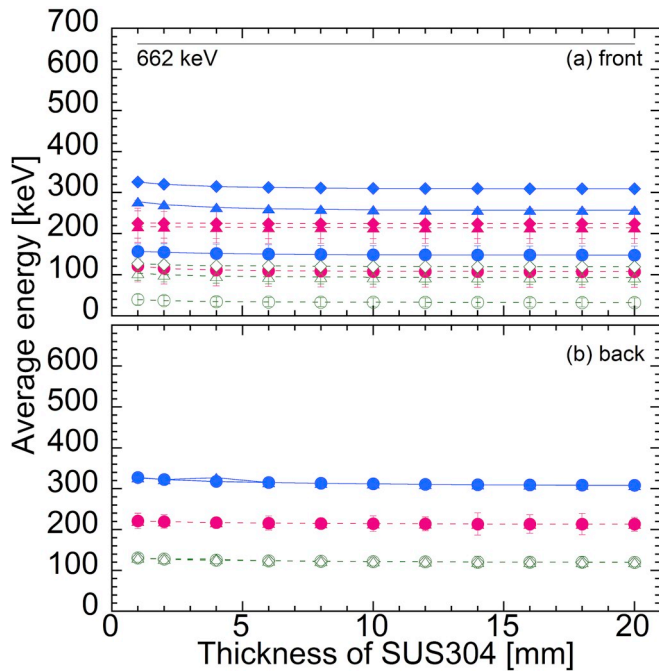


Fig. 5. Revised. Average energies of secondary radiations generated by gamma-ray from ^{137}Cs . (a) Front side. (b) Back side. The case of 0.0 mm spacing (circle), 0.5 mm (triangle) and 1.0 mm (diamond). The solid line denotes photon and the dotted line electron. The closed symbol denotes average energy of secondary radiations and the open symbol that of secondary and tertiary electrons (see text, Eq. (5)).

number of PHITS Monte Carlo simulation. According to the Compton scattering (1), the scattered energy, E' of photon becomes smaller than the incident one, E as its scattered angle, θ becomes larger.

$$E' = \frac{E}{1 + \frac{E}{m_e c^2} (1 - \cos\theta)} \quad (1)$$

where m_e denotes electron rest mass, c speed of light, and $m_e c^2$ 511 keV. In the case of ^{137}Cs γ -ray (662 keV), the scattered energy changes from 662 keV at $\theta = 0^\circ$ to 288 keV at $\theta = 90^\circ$ and 184 keV at 180° .

The peak and weighted center reflected the Compton back scattering at $\theta > 90^\circ$. The ratio to the photon flux at the peak for 1 mm-

thickness SUS304 increased with increasing the SUS304 thickness up to 2.30 ± 0.03 for 20 mm SUS304, reflecting the reflection of photon by SUS304. On the other hand, those did not depend almost on the spacing between the ^{137}Cs and SUS304. However, in Fig. 3a (c) and (e) at the spacing larger than 0.0 mm, a gap was observed at 180–185 keV together with the appearance of peak at 275–295 keV. In Fig. 3a (c) and (e), the flux did not depend on the thickness in the energy region higher than 180–185 keV, compared with that in Fig. 3a (d) and (f) at the back side. From this, it is considered that the photon spectra in the higher region at the front side reflect the interaction of incident photons. As discussed in the next paragraph, not only the primary radiation but also the secondary ones affected the spectra at the back side. The peak position at 275–295 keV somewhat depended on the spacing. The peak at 0.5 mm spacing was observed at 275–280 keV, corresponding to the deflection angle of $94\text{--}96^\circ$, while the peak at 1.0 mm at 290–295 keV, corresponding to that of $88\text{--}89^\circ$. The electron flux decreased sharply at the Compton edge of 475–485 keV in Fig. 3a (c) and (e) as shown in Table 1.

At the back side in Fig. 3a (b), (d), (f) and 4 (b), the energy spectra were almost the same, and no difference was observed due to the spacing. However, the dependence of the energy spectra on the thickness was clearly observed as the shielding effect of SUS304 against the incident γ -rays. According to the linear attenuation coefficient, the mean free path (MFP) of γ -ray of 662 keV in SUS304 is 16.8 mm (63% attenuation) as shown in Table 2. For example, in the case of 0.0 mm spacing in Fig. 3a (b), the total photon flux at 18 mm thickness was attenuated to $58.6 \pm 3.3\%$ of that at 1 mm (17 mm difference). Compared to the back side, the energy spectrum of the front side was small due to the increase of thickness, and almost no change was observed at 14 mm.

3.1.2. Average energy with ^{137}Cs γ -ray irradiation

The average energies of secondary radiations of photons and electrons generated from water and SUS304 were plotted as a function of the SUS304 thickness as shown in Fig. 5.

The average energies of photons and electrons, E_{av} (2) were evaluated from the energy spectra, each energy (e_i) and flux (f_i) as follows.

$$E_{av} = \frac{\sum_{i=1}^n e_i f_i}{\sum_{i=1}^n f_i} \quad (2)$$

At the front side (a), the E_{av} of photon (solid line), $E_{p_{av}}$ was the highest at the SUS304 thickness of 1 mm, and then monotonously

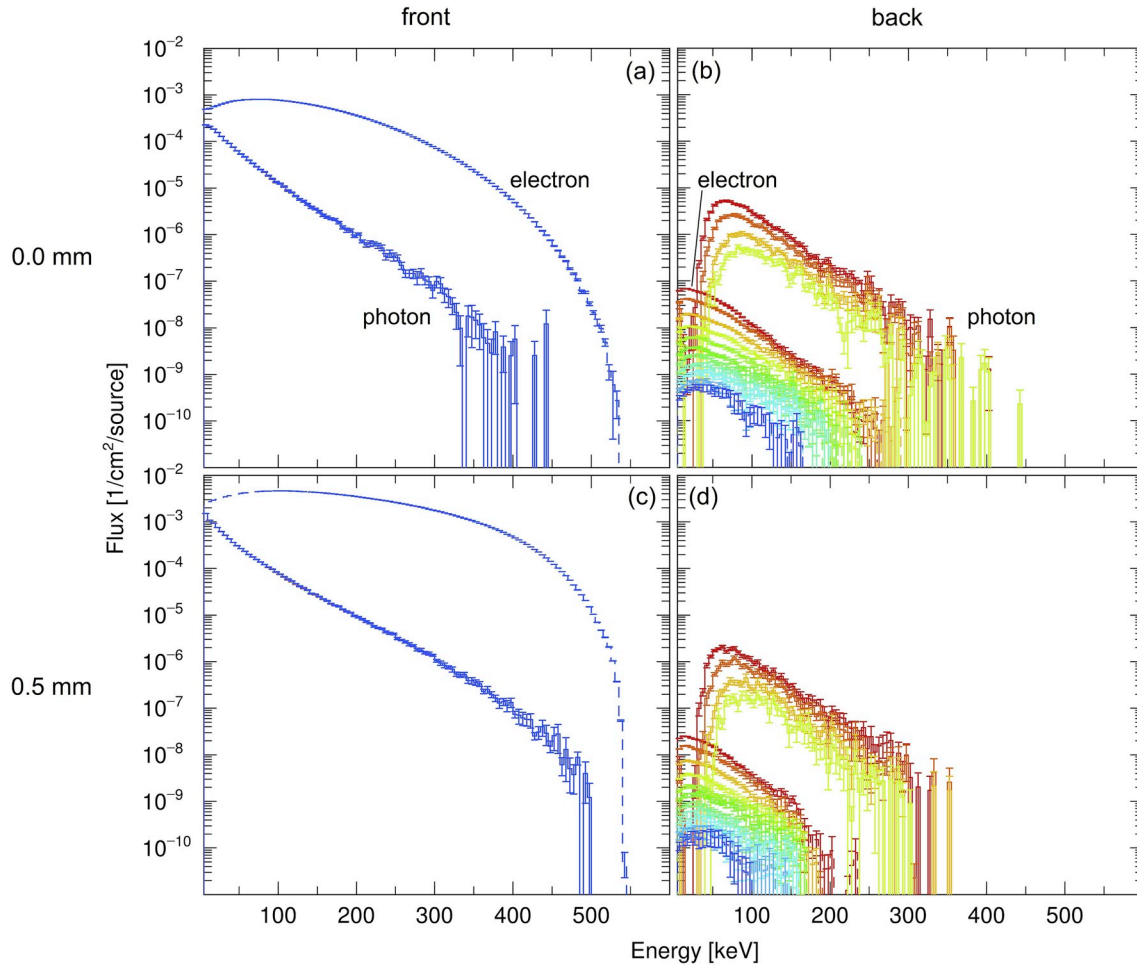


Fig. 6. Dependence of energy spectra of secondary radiations in water on SUS304 thickness and on spacing between beta-ray source of ^{90}Sr and SUS304. (a) and (c) were the front side at the spacing of 0.0 mm and 0.5 mm, respectively. (b) and (d) were the back side at 0.0 mm and 0.5 mm, respectively. The solid line denotes photon, and the dashed line electron. Line color is as shown in Fig. 3b. (For interpretation of the references to color in this figure legend, the reader is referred to the Web version of this article.)

decreased as the thickness increased. For example, the $E_{p,av}$ at the spacing of 1.0 mm was from 326 ± 2 keV at 1 mm thickness to 309 ± 2 keV at 20 mm thickness (5.2% decrease). The decrease can be considered to reflect the fact in Fig. 3a that at 1 mm thickness the flux of scattered photons in the lower energy region below 185 keV was minimum due to the poor reflection of photon and then that in the higher energy region increased relatively.

On the other hand, the $E_{p,av}$ increased with increasing the spacing from 0.0 mm to 1.0 mm. When the thickness was 1 mm, the energy was from 157 ± 19 keV at 0.0 mm spacing to 326 ± 2 keV at 1.0 mm where the radiation source was apart from SUS304 and then the peak at 275–295 keV appeared. The E_{av} of electrons, $E_{e,av}$ was lower than the $E_{p,av}$, and increased as the spacing increased, too. The $E_{e,av}$ was linked with the $E_{p,av}$ because electrons are mainly generated by the Compton scattering between photons and atom. The $E_{e,av}$ did not depend on the thickness, different from the $E_{p,av}$.

At the back side (b), the $E_{p,av}$ and $E_{e,av}$ were independent of the spacing at the front side. For example, in the case of 1 mm spacing the $E_{p,av}$ and $E_{e,av}$ at 1 mm thickness were 327 ± 2 keV and 221 ± 19 keV, respectively, while those at 20 mm thickness were 308 ± 3 keV and 213 ± 17 keV, respectively. Therefore, the energies decreased with increasing the thickness. However, the change in average energy was within 10%.

Since tertiary electrons generated from the interaction of secondary photons could be involved in water radiolysis, the average energy, $E_{p,av}$ of photon as mentioned above was further converted to that of electron.

Assuming that the interaction of photons was only the Compton scattering on the basis of the $E_{p,av}$ in Fig. 5, the average energy of electron generated by Compton scattering, $E_{e,comp}$ were evaluated from $E_{p,av}$ and $\gamma = \frac{E_{p,av}}{m_e c^2}$ (3, 4) as follows.

$$E_{e,comp} = E_{p,av} \left[1 - F_{p,comp} \right] \quad (3)$$

$$F_{p,comp} = \frac{\frac{4}{3} - \frac{3}{2\gamma} - \frac{1}{2\gamma(2\gamma+1)} + \frac{1}{\gamma} \ln(2\gamma+1) - \frac{1}{3(2\gamma+1)^3}}{\left[1 - \frac{2(\gamma+1)}{\gamma^2} \right] \ln(2\gamma+1) + \frac{1}{2} + \frac{4}{\gamma} - \frac{1}{2(2\gamma+1)^2}} \quad (4)$$

According to these equations, the average energy of the tertiary electrons is much smaller than the average energy of the secondary photons. For example, the photons with the average energy of 157–327 keV were converted to the electron with 29–92 keV. Assuming that all photons were converted to electrons in the observation region, the whole average energy of electrons, $E_{e,tav}$ (5) was evaluated from the $E_{e,av}$ of secondary electrons and the $E_{e,comp}$ of tertiary electrons as follows.

$$E_{e,tav} = \frac{E_{e,comp} \sum_{i=1}^n f_{p_i} + E_{e,av} \sum_{i=1}^n f_{e_i}}{\sum_{i=1}^n (f_{p_i} + f_{e_i})} \quad (5)$$

where the total flux ($\sum_{i=1}^n f_{p_i}$) of secondary photons and the total flux

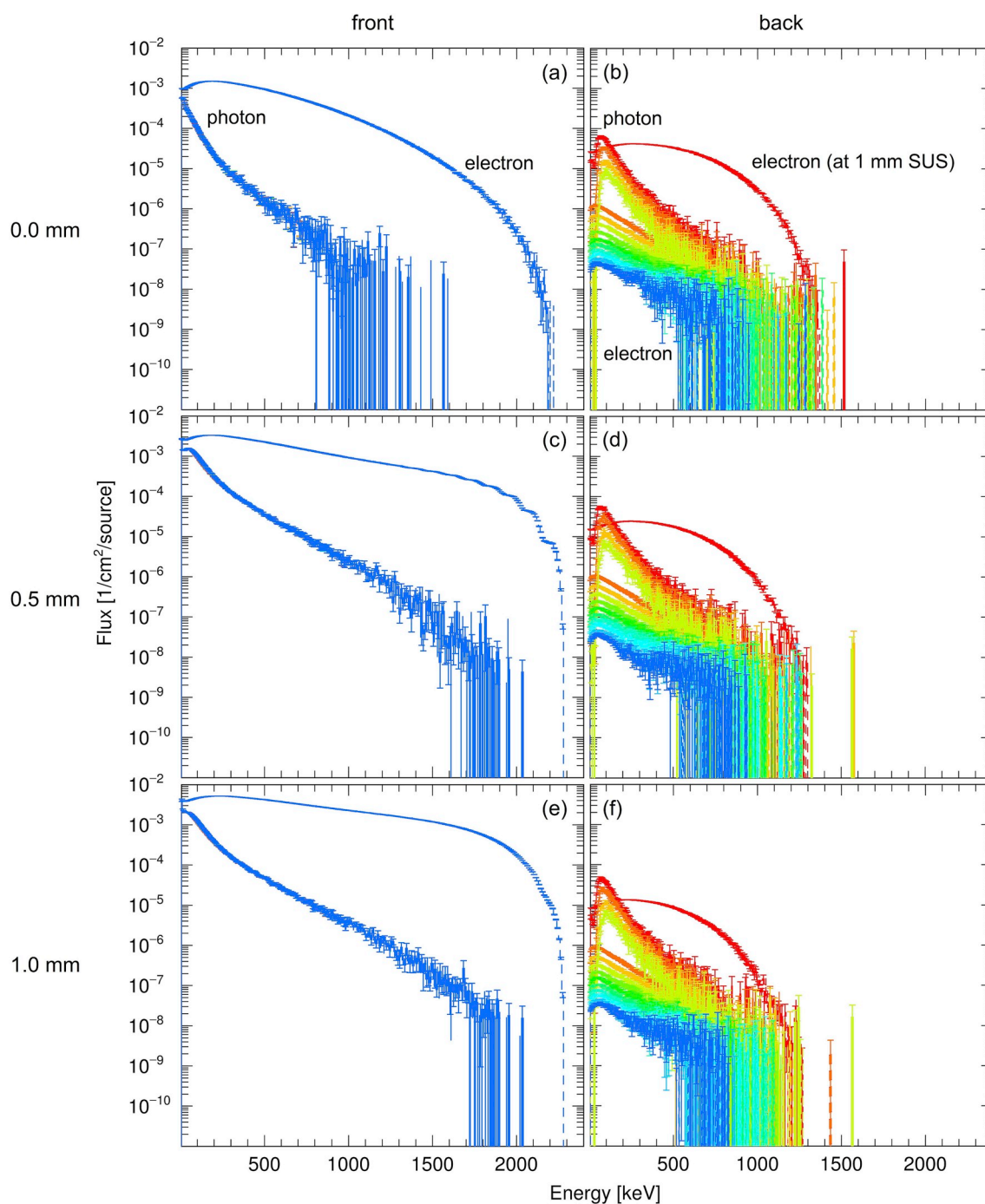


Fig. 7. Dependence of energy spectra of secondary radiations in water on SUS304 thickness and on spacing between beta-ray source of ^{90}Y and SUS304. (a), (c), and (e) were the front side at the spacing of 0.0 mm, 0.5 mm and 1.0 mm, respectively, (b), (d), and (f) were the back side at 0.0 mm, 0.5 mm and 1.0 mm, respectively. The solid line denotes photon, and the dashed line electron. Line color is as shown in Fig. 3b. (For interpretation of the references to color in this figure legend, the reader is referred to the Web version of this article.)

($\sum_{i=1}^n f_{ei}$) of secondary electrons. At both of the front and back sides, the $E_{e_{tav}}$ became significantly lower than those of the secondary and incident photons. In radiation chemistry of water, electron or photon of 0.1–20 MeV (Farhataziz et al., 1987), in which LET is within 0.18–2.0 eV/nm (Nagaishi et al., 2017), can be considered to give the same primary yields (G-value) of radiolysis products of water. The LET increases with decreasing the incident energy of radiations lower than 0.1 MeV. It can be noted that the electrons with the $E_{e_{tav}}$ would give the different G-values. For example, the G-value of H_2O_2 as an oxidizing agent increases with increasing the LET (LET effect).

3.2. Simulated calculation with β -ray irradiation

In this section, ^{90}Sr and ^{90}Y were selected as the β -ray sources. Since the range of β -ray in water is low, two types of the spacing of 0.0 mm and 0.5 mm were set in the simulation of β -ray from ^{90}Sr . The other conditions are the same as in the case of previous section 3.1.

3.2.1. Energy spectrum with ^{90}Sr and ^{90}Y β -ray irradiation

Figs. 6 and 7 show the energy spectra from SUS304 irradiated with β -rays from ^{90}Sr and ^{90}Y , respectively. The shapes at the front and back sides significantly changed with the spacing. However, the shapes due

to the change in the SUS304 thickness were clearly observed at the back side but not at all at the front side.

The energy spectra were clearly different from those of γ -ray. At the front side, the energy and flux of electrons were higher than those of photons. Also, the energy spectra of electrons and photons were not dependent on the thickness. At the back side, the energy and flux of electrons were lower than those of photons. On the other hand, the energy spectra of electrons and photons were dependent on the thickness. The electron flux decreased with increasing the energy more slowly than the photon one. When the incident β -rays are decelerated in the Coulombic field of atom in matter, the decelerated energy is also released as secondary photons of bremsstrahlung. Therefore, the maximum energy of photon is always distributed in matter with energy much lower than the maximum energy of incident β -ray.

At the front side in Fig. 6 (a) and (c), the electron flux decreased more slowly than the photon one with a maximum peak at 75–105 keV. The flux at 0.5 mm spacing reached to the energy region higher than those at 0.0 mm. Along with this, the photons were generated in the higher energy region up to around 500 keV. At the back side in Fig. 6 (b) and (d), the flux and energy of photon were higher than electron regardless of the spacing. It can be considered that the photon generated by the interaction of incident β -ray with water and SUS304 has higher permeability than electron to reaches into the back side. The photon flux decreased obviously with increasing the thickness, and then electrons generated from the photons were followed by the decreasing tendency.

At the front side in Fig. 7 (a), (c) and (e) for ^{90}Y , the energy spectra of electrons and photons behaved as in Fig. 6 for ^{90}Sr . At the back side in Fig. 7 (b), (d) and (f), the spectra of electrons only at 1 mm thickness was quite different from those in Fig. 6 (b) and (d) for ^{90}Sr . As shown in Table 2, it can be understood that a part of the incident β -rays from ^{90}Y penetrated the 1 mm-thickness SUS304.

3.2.2. Average energy with ^{90}Sr and ^{90}Y β -ray irradiation

The average energies of secondary radiations of photons and electrons generated from water and SUS304 by β -rays emitted from ^{90}Sr and ^{90}Y were shown in Figs. 8 and 9, respectively. As in previous section 3.2.1, the results for ^{90}Sr was discussed in the first half, and then those for ^{90}Y in the latter half.

At the front side in Fig. 8 (a), the average energies of electrons for all the spacing were almost independent of the SUS304 thickness. On the other hand, the average energy increased as the spacing increased from 0.0 mm to 0.5 mm. The average energy at 1 mm thickness was 122 ± 18 keV at 0.0 mm spacing, and 165 ± 8 keV at 0.5 mm. As shown in Fig. 6 (a) and (c), the increase of average energy with the spacing reflects the relative increase in the existence of electrons with higher energy. The average energies of photons (43 ± 30 keV) were much lower than those of electrons and independent of both of the thickness and spacing (MFP for the 43 keV photons was 39.3 mm in water). When the photon energy is lower than about 100 keV, both of the photoelectric effect and the Compton scattering occur at the same time. The proportion of Compton scattering for the 40 keV photons was nearly 80%. Therefore, the average energies of the tertiary electrons increase by a few keV compared to those evaluated only by Compton scattering.

At the back side in Fig. 8 (b), the average energies of electrons were much lower than those of photons and almost independent of the thickness, and slightly decreased with increasing the spacing. The average energy at 0.5 mm spacing was 49 ± 16 keV at 1 mm thickness and 45 ± 6 keV at 20 mm. On the contrary, the photons clearly showed the dependence on the thickness. The average energy at 0.5 mm spacing was 93 ± 29 keV at 1 mm thickness and 129 ± 19 keV at 20 mm. The increase of average energy with the thickness showed that the photon at lower energy was shielded (absorbed) by SUS304 more than that at higher energy so that the average energy became high. Then the average energies of electrons generated from the photons was followed

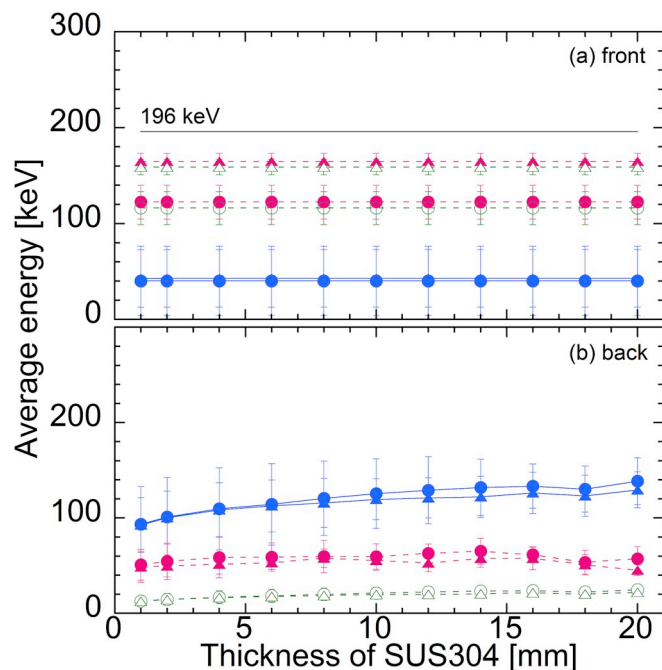


Fig. 8. Revised. Average energies of secondary and tertiary radiations generated by beta-ray emitted from ^{90}Sr . (a) Front side. (b) Back side. The case of 0.0 mm spacing (circle) and 0.5 mm (triangle). The solid line denotes photon and the dotted line electron. The closed symbol denotes secondary radiations and the open symbol tertiary radiations (see text in 3.1.2).

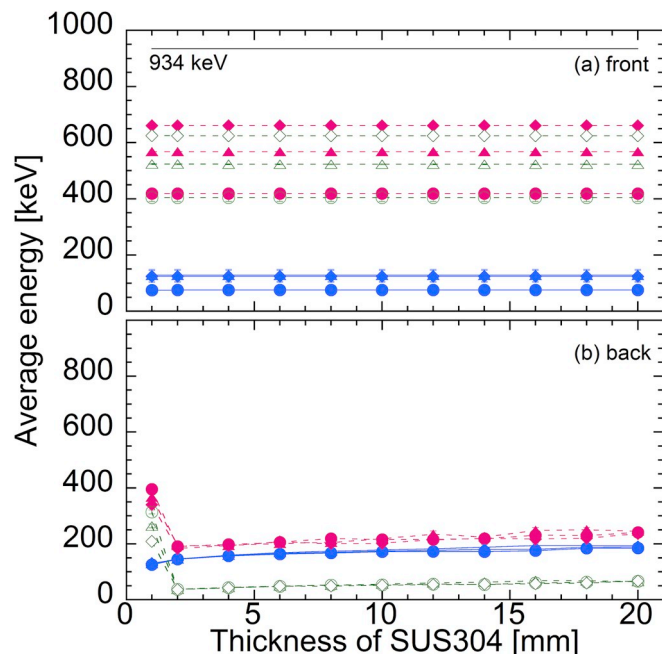


Fig. 9. Revised. Average energies of secondary and tertiary radiations generated by beta-ray emitted from ^{90}Y . (a) Front side. (b) Back side. The case of 0.0 mm spacing (circle), 0.5 mm (triangle) and 1.0 mm (diamond). The solid line denotes photon and the dotted line electron. The closed symbol denotes secondary radiations and the open symbol tertiary radiations (see text in 3.1.2).

by the variation in the average energies of photons as mentioned above.

At the front side in Fig. 9 (a), the average energies of electrons and photons gave similar results to those in Fig. 8 (a). The average energy of electron at 1 mm thickness was 419 ± 14 keV at 0.0 mm spacing and 661 ± 2 keV at 1.0 mm, while that of photon was 75 ± 14 keV at

0.0 mm and 124 ± 21 keV at 1.0 mm. At the back side in Fig. 9 (b), the result only at 1 mm thickness became different from that for ^{90}Sr . This is because the maximum energy of the β -ray from ^{90}Y is 2284 keV and the CSDA range in SUS304 is 1.94 mm. Therefore, it was considered that in the case of the 1 mm-thickness SUS304, a part of the electrons of β -rays passed through the SUS304. In the case of the average energy at the thickness larger than 1 mm, the energies of electrons became higher than those of photons unlike ^{90}Sr . This was because there were electrons in the higher energy region relatively more than those in the lower energy region according to eq. (2). When the spacing between the source and the SUS304 is 0.0 mm, the proportion of Compton scattering for the 75 keV photon was nearly 90%. Therefore, the average energies of tertiary electrons increased by a few keV compared to those evaluated only by Compton scattering.

Although ^{90}Sr and ^{90}Y were selected as the β -ray sources in this work, β -rays are also emitted from the γ -ray sources of ^{137}Cs and ^{134}Cs . These average energies (187 (^{137}Cs) and 157 (^{134}Cs) keV) are nearly corresponding to that from ^{90}Sr (196 keV). These β -rays are consequently suggested to give similar results to that from ^{90}Sr .

4. Conclusion

The energy spectra of secondary radiations of photons and electrons at the front and back sides of SUS304 plate in water were simulated by using a Monte Carlo calculation code of PHITS.

In the case of ^{137}Cs γ -ray (662 keV), the $E_{p_{av}}$ and $E_{e_{av}}$ at the front side were nearly independent of the SUS304 thickness. On the other hand, the $E_{p_{av}}$ and $E_{e_{av}}$ at a constant 1 mm thickness decreased from 326 ± 2 keV and 226 ± 37 keV at 1.0 mm spacing to 157 ± 19 keV and 121 ± 38 keV at 0.0 mm, respectively. However, the total flux did not depend on the thickness. At the back side, the $E_{p_{av}}$ and $E_{e_{av}}$ were independent of the spacing at the front side, and were 327 ± 2 keV and 221 ± 19 keV at 1 mm thickness, respectively. The change of $E_{p_{av}}$ and $E_{e_{av}}$ to the thickness were within 10%. However, the total flux was dependent largely on the thickness. The whole energy of electrons involved in water radiolysis became significantly lower than the primary and secondary photons.

Practically in a pitting test, a test sample plate is put into a cylindrical vessel satisfied with water and irradiated externally by ^{60}Co γ -ray. The size (diameter) of vessel in this case is corresponding to the spacing between the radiation source and SUS304 in this work. When the vessel size changes, the test results would change as mentioned above.

In the case of ^{90}Sr and ^{90}Y β -ray (maximum 546 and 2284 keV), the $E_{e_{av}}$ and $E_{p_{av}}$ for all the spacing at the front side were almost independent of the thickness. On the other hand, the $E_{e_{av}}$ decreased as the spacing decreased while $E_{p_{av}}$ were almost independent. The $E_{e_{av}}$ at 1 mm thickness decreased with decreasing the spacing from 165 ± 8 keV to 122 ± 18 keV for ^{90}Sr , and from 661 ± 2 keV to 419 ± 14 keV for ^{90}Y . At the back side, the $E_{e_{av}}$ and $E_{p_{av}}$ for all the thickness were almost independent of the spacing oppositely. The $E_{e_{av}}$ for ^{90}Sr at 1 mm thickness was 51 ± 16 keV. The $E_{p_{av}}$ at 0 mm spacing increased from 93 ± 40 keV to 139 ± 25 keV as the thickness increased. In the case of ^{90}Y , both of the $E_{e_{av}}$ and $E_{p_{av}}$ increased with the thickness. The $E_{e_{av}}$ and $E_{p_{av}}$ increased from 191 ± 14 keV to

241 ± 9 keV and from 145 ± 12 keV to 185 ± 6 keV at 2 mm thickness, respectively.

From the above results, it was clearly shown how the energy spectra and average energies of secondary radiations varied with the incident radiation type, the spacing between radiation source and SUS304, and the plate thickness. And the energies of electrons that gives energy to water became significantly lower than the incident γ -rays and β -rays. Therefore, there is a possibility that the electrons with the lower energies give different primary yields of radiolysis products of water. This work will be helpful for studying the corrosion and degradation of structural materials in radiation fields.

Acknowledgements

I am grateful to M. Fujita and S. Abe for useful technical advices and discussions on the PHITS simulation.

References

- Allen, A.O., 1961. Radiation Chemistry of Water and Aqueous Solution. D. Van Nostrand.
- Bethe, H.A., et al., 1934. On the stopping of fast particles and the creation of positive electrons. Proc. R. Soc. London, Ser. A 146, 83.
- Eckerman, K.F., et al., 1994. Availability of nuclear decay data in electronic form, including beta spectra not previously published. Health Phys. 67 (4), 338–345.
- ESTAR program < <https://physics.nist.gov/PhysRefData/Star/Text/ESTAR.html> > .
- Farhataziz, et al., 1987. Radiation Chemistry Principles and Applications. VCH Publishers, Inc.
- Hanawa, S., et al., 2010. ECP measurements under neutron and gamma ray in in-pile loop and their data evaluation by water radiolysis calculations. In: Proceedings of Nuclear Plant Chemistry Conference (NPC2010). Canada, Quebec City, pp. 10p in CD-ROM.
- Heitler, W., et al., 1954. The Quantum Theory of Radiation. Clarendon Press, Oxford.
- Hubbell, J.H., et al., 1995. "Tables of X-ray Mass Attenuation Coefficients and Mass Energy-Absorption Coefficients from 1 keV to 20 MeV for Elements Z = 1 to 92 and 48 Additional Substances of Dosimetric Interest", NISTIR 5632. National Institute of Standards and Technology.
- Itoh, N., 1988. Bachelor thesis. Nucl. Eng. Dept., Univ. of Tokyo.
- JIS G 0577, 2014. 2014, "Methods of Pitting Potential Measurement for Stainless Steels.
- JIS G 0578, 2013. 2013, "Method of Ferric Chloride Tests for Stainless Steels.
- JIS G 0590, 2013. 2013, "Method of Critical Pitting Temperature Measurement for Stainless Steels.
- John Sedriks, A., et al., 1979. Corrosion of Stainless Steels. Wiley.
- Katakura, J., et al., 2016. "JENDL Decay Data File 2015", JAEA-Data/code 2015-030. JAEA.
- Klein, O., et al., 1929. Über die streuung von strahlung durch freie electronen nach der neuen relativistischen quantendynamik von Dirac. Z. Phys. 52, 853–868.
- Matsumura, T., et al., 2018. Analytical studies of three-dimensional evaluation of radionuclide distribution in zeolite wastes through gamma scanning of adsorption vessels. Nucl. Sci. Eng. 192, 70–79.
- Nagaishi, R., et al., 2014. Consideration of radiolytic behavior in diluted and concentrated systems of seawater for computational simulation of hydrogen generation. In: Proceedings of 2014 Nuclear Plant Chemistry Conference (NPC 2014) (USB Flash Drive), vol. 9.
- Nagaishi, R., et al., 2017. Modern radiation chemistry (applications), 26; evolution of water radiolysis studies for measures against post-severe accidents. Radioisotopes 66, 601–610.
- Okumura, K., et al., 2013. Nuclear data for severe accident analysis and decommissioning of nuclear power plant. In: JAEA-conf 2013-002.
- PHOTX, 1995. Photon Interaction Cross-Section Library for 100 Elements. Data Package DLC-136/PHOTX, Radiation Shielding Information Center. Oak Ridge National Laboratory, Oak Ridge, TN.
- Sato, T., et al., 2018. Features of particle and Heavy ion Transport code System PHITS version 3.02. J. Nucl. Sci. Technol. 55, 684–690.
- Takagi, J., et al., 1985. Thermal decomposition of hydrogen peroxide and its effect on reactor water monitoring of boiling water reactors. Nucl. Sci. Eng. 89, 177–186.